Proceedings of the 2016 IEEE
International Conference on Robotics and Biomimetics
Qingdao, China, December 3-7, 2016

3D Evolutionary Pose Tracking Experiments of Eye-Vergence Visual Servoing in Lateral Motion and Arc Swing Motion

Hongzhi Tian[1], Ryuki Funakubo, Yejun Kou and Mamoru Minami

***Abstract*— The moving target visual servoing with hand eye cameras fixed at hand is inevitably affected by dynamic oscillatory, so that it's difficult to remain target position at the center of the camera's view, because the tracing ability of the system is influenced by non-linear dynamics of the entire manipulator. To overcome this defect of the fixed hand-eye system, hand-eye-vergence system in which left and right cameras' directions could be rotated to observe and keep the target object to be seen at the center of camera images to reduce the influences of aberration of camera lens. This paper analyses the performance of 3D-object position and orientation tracking experiments of hand-eye-vergence system. They both show good tracking performance. In this paper an orientation recognition method using quaternion is put forward. And quaternion is incorporated into chromosomes and participates in the evolution of Genetic Algorithms (GA). The dynamical superiorities of the proposed system are verified by comparing hand tracking performances and the proposed eye-vergence tracking performances in two experiments of lateral and arc swing motion respectively.**

I. Introduction

The visual servoing, a method for controlling a robot using visual information in the feedback loop, is expected to be able to allow the robot to adapt to changing or unknown environments [1]. Some methods have already been proposed to improve observation abilities, by using stereo cameras [2], multiple cameras [3], and two cameras; with one fixed on the end-effector and the other one fixed in the workspace [4]. These methods obtain multiple different views to observe an object by increasing the number of cameras.

When the end-effector is close to a target object, eye-vergence camera system can look at it in the center of camera images all the time by utilizing the changeable cameras' eye directions [5]. Therefore in the future the system can be made for getting up the end-effector to a target object while watching it. And about another advantage when the object become moving faster and faster, human's face can hardly keep position squarely to the object, while human's eye can still keep staring at the object because of its small mass and inertial moment. In this report the merits of eye-vergence visual servoing for tracking have been confirmed experimentally by using eye-vergence function that enables the target to be seen at the center of images, avoiding influences of aberration of lens.

For the pose tracking of 3D objects, we design two experiments in which target takes lateral motion and swing motion along the arc for testing positon and orientation tracking ability of proposed system. In the former research [6] we just proposed orientation recognition method based on eye-vergence system. In this paper we design new experiment to research the performance of orientation recognition method. From the results of experiments, it is clear that the proposed eye-vergence system has stable tracking ability confirmed by pose tracking frequency experiment where a target with 3D-pose moves periodically.

There are other methods for identifying moving objects from a video sequence such as frame difference, background subtraction and optical flow three methods [7]. However they are sensitive to background. We use model-based matching method [8]. It is sensitive to the changing of background.

This paper about eye-vergence visual servoing is basic research. Interested readers is referred to [9] for details about the application of the study.

[1]Hongzhi Tian is with Division of Mechanical and Systems Engineering, Graduate school of Natural Science and Technology, Okayama University, 1-1-1 Tsushima-naka, Kita-ku, Okayama 700-8530, Japan psnc8ytd@s.okayama-u.ac.jp

II. 3D POSE TRACKING METHOD

In this paper, a 3D-ball-object as shown in Fig.5(d) is used as 3D target object whose size and color are known.

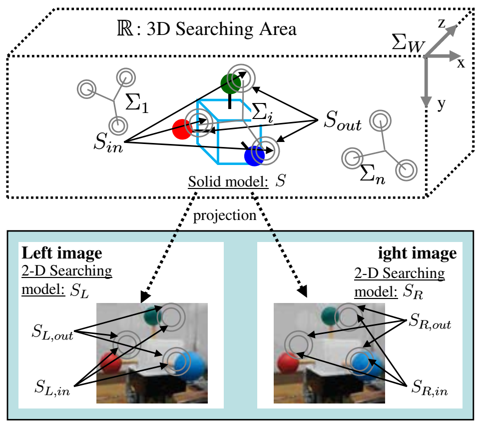

Fig. 1. Definition of a solid model and left/right searching models

A. Model-Based Recognition Using Real-Time Multi-Step GA

In [8] dual-camera eye-vergence approach have been described in detail, the following is summarized explanation about real time pose tracking method. The 3D solid model named S of a rectangular block is shown in Fig.1 (on the top). The set of coordinates inside of the dotted line block named $\mathbb{R}$ in Fig.1 means searching space where pose tracking is conducted on an assumption that the 3D marker in Fig.5(d) exist in the space $\mathbb{R}$.

The model to detect 3D-ball-object has the same 3D structure with the 3D-ball-object. The model is represented in $\mathbb{R}$ by three double circles with light color, where inside of inner wide is named as S_{in}, and space between S_{in} and outer circle is named S_{out}.

The i-th 3D model is represented by Σ_i, whose pose is assumed to the defined by chromosome

$$\overbrace{\underbrace{10\cdots10}_{12bit}}^{t_x}\overbrace{\underbrace{11\cdots01}_{12bit}}^{t_y}\overbrace{\underbrace{01\cdots10}_{12bit}}^{t_z}\overbrace{\underbrace{11\cdots10}_{12bit}}^{\varepsilon_1}\overbrace{\underbrace{10\cdots10}_{12bit}}^{\varepsilon_2}\overbrace{\underbrace{10\cdots01}_{12bit}}^{\varepsilon_3}.$$

Since the number of chromosome is n, S_{in} and S_{out} are renamed as $S_{in,k}$, $S_{out,k}(k = 1, 2, \cdots, n)$. Note that the 3D model composed of $S_{in,k}$ and $S_{out,k}$ are 3D model, the sizes of the balls projected into 2D image of left camera and right one from 3D model are different since the camera depth distance of each ball is different in 3D space $\mathbb{R}$ in Fig.1. Projecting S_{in} and S_{out} onto the 2D coordinates of left camera Σ_{IL} and right camera Σ_{IR}, the left and right 2D searching models, named S_L and S_R, are calculated and shown in Fig.1(on the bottom). Color information is used to search for the target object in the images. Supposing there are distributed solid models in the searching space in Σ_W, each has its own pose. To determine which solid model is most close to the real target, a correlation function used fitness function in Genetic Algorithm (GA) is defined for evaluation. Everyone of S_{in} have three small circles. And everyone of S_{out} have three 3 rings. The relative positions of circles and rings are unchanged. Each pair of circle and ring corresponds with a color, and three pairs of circles and rings are corresponding to red, blue and green. The higher coincidence degree between a circle and corresponding color ball is, the higher fitness is. Conversely, the higher coincidence degree between a ring and the corresponding color ball is, lower fitness will be. When the searching model fits to the target object being imaged in the right and left images, then the fitness function gives maximum value. This optimization problem is solved by GA. Detail discussion about Real-Time Multi-Step GA (RT-MS GA) is explained in [8], [9].

B. Orientation Recognition Method Using Quaternion

For representating the orientation of 3D object, widely used methods include Euler angles, Angle-axis representation and rotation quaternions. The first two methods are easy to understand. However, because the orientation singularities exist in the representation method of Euler angle and Angle-axis, in our system quaternion representation [10] has been adopted. The definition of unit quaternion is shown in Fig.2. On the basis of axis-angle representation, a unit vector $\boldsymbol{k}$ indicating direction, and an angle θ describing the magnitude of rotation around the axis. By using $\boldsymbol{k}$ and θ, quaternion set $\boldsymbol{q} = \{\eta, \boldsymbol{\varepsilon}\}$, $\boldsymbol{q}$ is defined as follows,

$$\boldsymbol{\varepsilon} = sin\frac{\theta}{2}\boldsymbol{k}, \tag{1}$$

in detail,

$$\left[\varepsilon_1, \varepsilon_2, \varepsilon_3\right]^T = sin\frac{\theta}{2}\left[k_x, k_y, k_z\right]^T. \tag{2}$$

η is the scalar part of the quaternion, and $\boldsymbol{\varepsilon}$ is the vector part of the quaternion. They satisfy the following relationship of unit quaternion:

$$\eta^2 + \boldsymbol{\varepsilon}^{\boldsymbol{T}}\boldsymbol{\varepsilon} = 1. \tag{3}$$

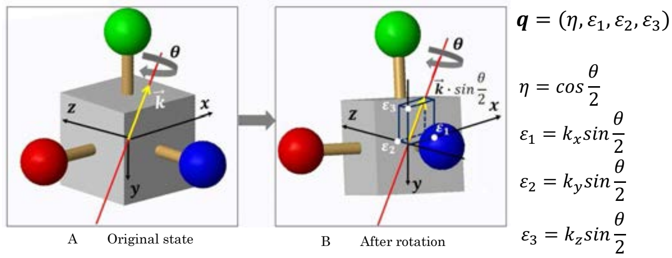

Fig. 2. Defination of quaternion in the proposed system.

It is worth remarking that, differently from the angle/axis representation, a rotation by an angle $-\theta$ about an axis $-\boldsymbol{k}$ gives the same quaternion as that associated with a rotation by θ about $\boldsymbol{k}$ which solves the non-uniqueness problem.

III. HAND & EYE VISUAL SERVOING CONTROLLER

A. Hand Visual Servoing Controller

The block diagram of our proposed hand & eye-vergence visual servoing controller is shown in Fig.3. The hand-visual servoing is the outer loop. Based on the above analysis of

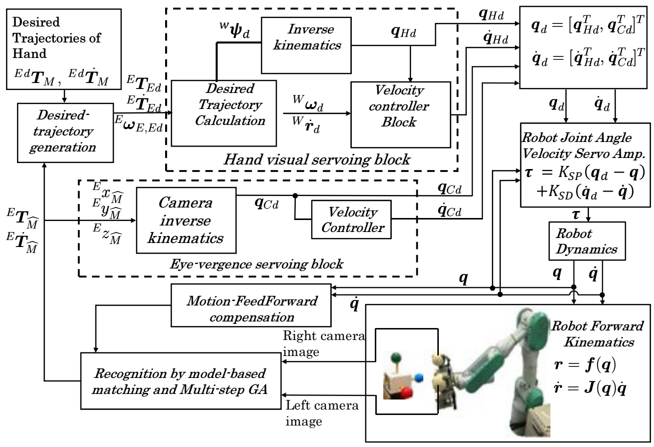

Fig. 3. Block diagram of the hand visual servoing system

the desired-trajectory generation, the desired hand velocity ${}^W\dot{\boldsymbol{r}}_d$ is calculated as,

$${}^W\dot{\boldsymbol{r}}_d = \boldsymbol{K}_{PP}{}^W\boldsymbol{r}_{E,Ed} + \boldsymbol{K}_{VP}{}^W\dot{\boldsymbol{r}}_{E,Ed}, \tag{4}$$

where ${}^W\boldsymbol{r}_{E,Ed}$, ${}^W\dot{\boldsymbol{r}}_{E,Ed}$ can be calculated from ${}^E\boldsymbol{T}_{Ed}$ and ${}^E\dot{\boldsymbol{T}}_{Ed}$. $\boldsymbol{K}_{PP}$ and $\boldsymbol{K}_{VP}$ are positive definite matrix to determine PD gain.

The desired hand angular velocity ${}^W\boldsymbol{\omega}_d$ is calculated as,

$${}^W\boldsymbol{\omega}_d = \boldsymbol{K}_{PO}{}^W\boldsymbol{R}_E{}^E\Delta\boldsymbol{\varepsilon} + \boldsymbol{K}_{VO}{}^W\boldsymbol{\omega}_{E,Ed}, \tag{5}$$

where ${}^E\Delta\boldsymbol{\varepsilon}$ is a quaternion error [10] calculated from the pose tracking result, and ${}^W\boldsymbol{\omega}_{E,Ed}$ can be computed by transforming the base coordinates of ${}^E\boldsymbol{T}_{Ed}$ and ${}^E\dot{\boldsymbol{T}}_{Ed}$ from Σ_E to Σ_W. Also, $\boldsymbol{K}_{PO}$ and $\boldsymbol{K}_{VO}$ are suitable feedback matrix gains. The desired hand pose is defined as

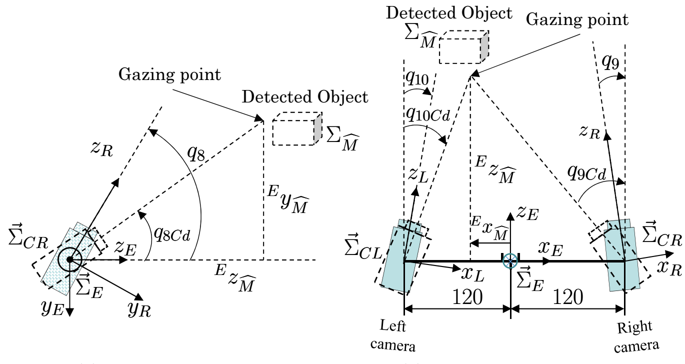

(a) Tilt angle q_8 (b) Pan angle q_9 and q_{10}

Fig. 4. Definition of tilt and pan angles with relation of detected object

${}^W\boldsymbol{\psi}_d = [{}^W\boldsymbol{r}_d^T, {}^W\boldsymbol{\varepsilon}_d^T]^T$. And the desired joint variable $\boldsymbol{q}_{Ed} = [0, q_{1d}, \ldots, q_{7d}]^T$ and $\dot{\boldsymbol{q}}_{Ed}$ is obtained by

$$\boldsymbol{q}_H = \boldsymbol{f}^{-1}({}^W\boldsymbol{\psi}), \boldsymbol{q}_{Hd} = \boldsymbol{f}^{-1}({}^W\boldsymbol{\psi}_d) \tag{6}$$

$$\dot{\boldsymbol{q}}_{Ed} = K_{PQ}(\boldsymbol{q}_{Hd} - \boldsymbol{q}_H) + \boldsymbol{J}_E^+(\boldsymbol{q}) \begin{bmatrix} {}^W\dot{\boldsymbol{r}}_d \\ {}^W\boldsymbol{\omega}_d \end{bmatrix} \tag{7}$$

where ${}^W\boldsymbol{\psi}$ is measured by RT-MS GA [8], [9]. $\boldsymbol{f}^{-1}({}^W\boldsymbol{\psi})$ is the inverse kinematic function and $\boldsymbol{J}_E^+(\boldsymbol{q})$ is the pseudo-inverse matrix of $\boldsymbol{J}_E(\boldsymbol{q})$, which is the Jacobian about joint angles $\boldsymbol{q}$, and $\boldsymbol{J}_E^+(\boldsymbol{q}) = \boldsymbol{J}_E^T(\boldsymbol{J}_E\boldsymbol{J}_E^T)^{-1}$.

The manipulator is 7 links, and the end-effector has 6-DoF, so q_1 is set as 0 to remove the redundancy of the robot PA 10. Using the inverse kinematics it can make the joint of angles approximately as the desired joint angles. The formula of the desired joint angles was defined in the new controller as

$$\dot{\boldsymbol{q}}_{Ed} = \boldsymbol{K}_P(\boldsymbol{q}_{Ed} - \boldsymbol{q}_E) + \boldsymbol{J}_E^+(\boldsymbol{q}) \begin{bmatrix} {}^W\dot{\boldsymbol{r}}_d \\ {}^W\boldsymbol{\omega}_d \end{bmatrix} \tag{8}$$

where $\boldsymbol{K}_P$ is positive gain.

The hardware control system of the velocity-based servo system of PA10 is expressed as

$$\boldsymbol{\tau} = \boldsymbol{K}_{SP}(\boldsymbol{q}_d - \boldsymbol{q}) + \boldsymbol{K}_{SD}(\dot{\boldsymbol{q}}_d - \dot{\boldsymbol{q}}) \tag{9}$$

where $\boldsymbol{K}_{SP}$ and $\boldsymbol{K}_{SD}$ are symmetric positive definite matrices to determine PD gain.

B. Eye-Vergence Visual Servoing Controller

The eye-vergence visual servoing is conducted by the inner loop of the visual servoing system shown in Fig.3. In this paper, two pan-tilt cameras are used for eye-vergence visual servoing. Here, the positions of cameras are supposed to be fixed on the end-effector. For camera system, q_8 is tilt angle, q_9 and q_{10} are pan angles, and q_8 is common for both cameras.

As it is shown in Fig.4 (a) and (b), ${}^Ex_{\widehat{M}}$, ${}^Ey_{\widehat{M}}$, ${}^Ez_{\widehat{M}}$ express position of the detected object in the end-effector coordinate. The desired angle of camera joints are calculated by:

$$q_{8Cd} = atan2({}^Ey_{\widehat{M}}, {}^Ez_{\widehat{M}}) \tag{10}$$

$$q_{9Cd} = atan2(l_{8R} - {}^Ex_{\widehat{M}}, {}^Ez_{\widehat{M}}) \tag{11}$$

$$q_{10Cd} = atan2(l_{8L} + {}^Ex_{\widehat{M}}, {}^Ez_{\widehat{M}}) \tag{12}$$

where $l_{8L} = l_{8R} = 120[mm]$ that is the camera location. The controller of eye-visual servoing is given by

$$\dot{q}_{iCd} = K_P(q_{iCd} - q_i) \qquad (i = 8, 9, 10) \tag{13}$$

where K_P is spring constant. $\dot{q}_{iCd}$ is input into pulse motors for the cameras' angle control as a pulse array.

Because the motion of camera motor is an open loop, it is controlled to rotate a certain degree without getting the actual angle during the rotation, which make the accurate camera angle cannot be got. So the desired camera angles gotten by GA recognition are input in every 33ms , and the input is limited to a certain value.

IV. EXPERIMENT OF HAND & EYE-VERGENCE VISUAL SERVOING

A. Experimental System

To verify the effectiveness of the hand & eye visual servoing system through real robot-PA-10 robot arm-manufactured by Mitsubishi Heavy Industries. And two rotatable cameras mounted on the end-effector are FCB-1X11A manufactured by Sony Industries. The frame frequency of stereo cameras is set as 30fps. The image processing board, CT-3001, receiving the image from the CCD camera is connected to the host computer (CPU: Intel Core i7-3770 , 3.40 GHz).

The structure of the manipulator and the cameras are shown in Fig.5. The coordinate of the target object and the manipulator in experiment are shown in Fig.6.

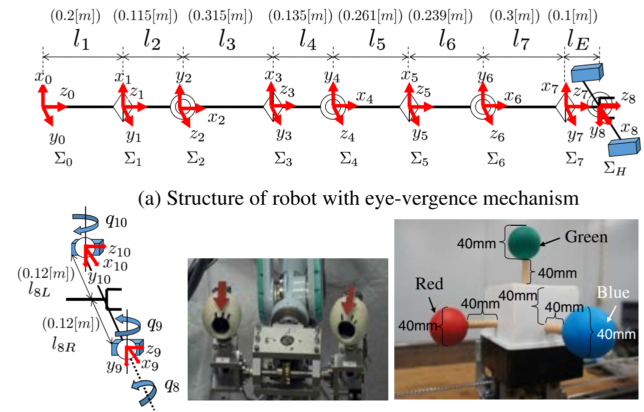

(a) Structure of robot with eye-vergence mechanism

(b) Eye-vergence mechanism (c) Photo of Eye-vergence (d) 3D target marker

Fig. 5. Frame structure of manipulator

B. Lateral Motion Experiment

1) Lateral Motion Experiment Condition: EO, MO and EC represent initial hand pose, initial object pose and mid-point of round-trip tracking movements of hand respectively. Therefore their coordinate systems are defined as Σ_{EO}, Σ_{EC} and Σ_{MO} separately and are shown in Fig.6 and 7. Target object motion function is

$$^{MO}z_M(t) = 150 - 150\cos(\omega t)[mm]. \tag{14}$$

Target position and orientation relationship between the object and the end-effector is set as:

$$^{Ed}\boldsymbol{\psi}_M = [0, -100[mm], 545[mm], 0, 0, 0]. \tag{15}$$

The object is subjected to reciprocating motion of the sine wave in orbit. Pose relationship of the coordinate system of

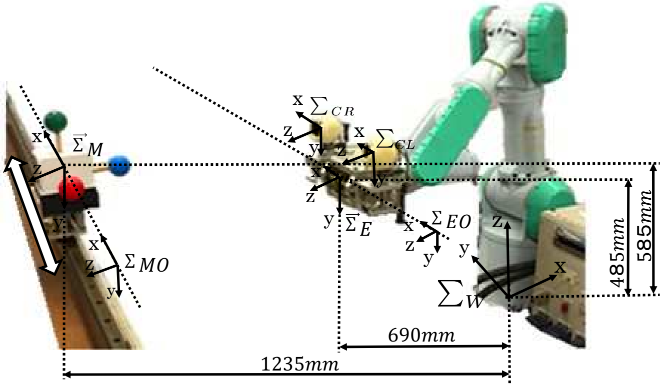

Fig. 6. Object and the visual-servoing system

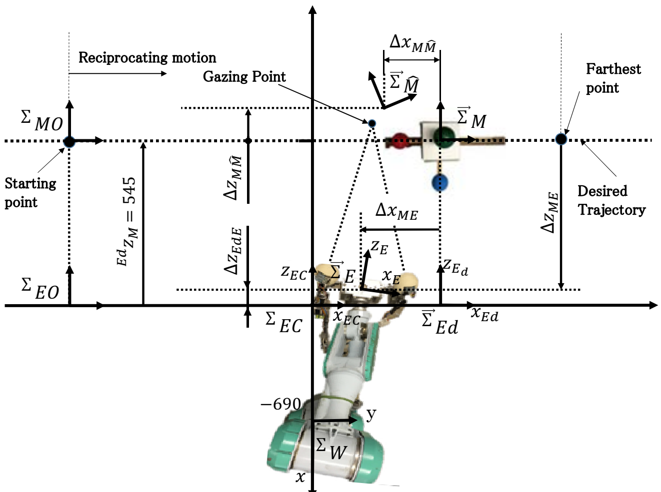

Fig. 7. Object is reciprocating on the trajectory in lateral direction. Object and the system are shown from the x-z plane of Σ_{EC} of hand. Initial position of the object Σ_{MO}, actual object $\vec{\Sigma}_M$, detected object $\vec{\Sigma}_{\widehat{M}}$, initial position of the hand Σ_{EO}, actual end effector $\vec{\Sigma}_E$ and theoretical end effector Σ_{Ed}. At this moment orientation $\varepsilon \neq 0$ since orientation of Σ_E and the one of $\vec{\Sigma}_M$ is different. $\Delta i_{ME} = {}^{EC}i_M - {}^{EC}i_E, \Delta i_{M\widehat{M}} = {}^{EC}i_M - {}^{EC}i_{\widehat{M}}, \Delta i_{EdE} = {}^{EC}i_{Ed} - {}^{EC}i_E$, $(i = x, y, z)$

the object and the visual servoing system is shown in Fig.6.

2) Symbol Meaning: M represents the object and $\widehat{M}$ represents the estimated object. Then $\vec{\Sigma}_M$ denotes the coordinate system that moves along with the object. The relationship between coordinate systems such as the actual pose of the hand $\vec{\Sigma}_E$ or the recognized pose of the object $\vec{\Sigma}_{\widehat{M}}$ which is viewed from the x-z plane of the center coordinate system Σ_{EC} is shown in Fig.7. In the figure $\vec{\Sigma}$ represents a coordinate system moving in the world coordinate system Σ_W. The coordinate system represented by Σ keeps fixed in Σ_W. In other words $\vec{\Sigma}_E$, $\vec{\Sigma}_{Ed}$, $\vec{\Sigma}_M$ and $\vec{\Sigma}_{\widehat{M}}$are all moving in Σ_W. On the other hand Σ_{EO}, Σ_{EC} and Σ_{MO} keeps fixed in the world coordinate system Σ_W. The motion of object M, hand E and gazing point $\widehat{M}$ in the x-axis direction of Σ_{EC} are represented by ${}^{EC}x_M$, ${}^{EC}x_E$ and ${}^{EC}x_{\widehat{M}}$. In the previous research [11] the gazing point was not defined as the left and right eye-sight line intersection but as the intersection of sight line of left camera and the $x_{MO} - y_{MO}$ plane in Σ_{MO} in Fig.6, so was right camera. Therefore there were two gazing points. This defination is very different with human eyes. To mimic human-eye system as shown in Fig.8, the intersection of both cameras' gazing directions is defined as the gazing point of cameras to examine trackability of the eye-vergence system. Because the gazing point has been calculated on the basis of the recognition result of the object by the multi-step GA, recognition error is included in the estimated Gazing point.

3) Lateral Motion Experiment Results:

a) Relation between position diagram and real machine: Fig.9 shows the positional relationship between the hand and the object in the condition that the tracking all the six position and orientation variables are recognized. And the motion period of the object is $T = 20$[s]. Movement trajectory of the object M, hand E and gazing point $\widehat{M}$ are represented by dashed line ${}^{EC}x_M$, dotted line ${}^{EC}x_E$ and solid line ${}^{EC}x_{\widehat{M}}$ respectively. At the time of Fig.9 (b) the hand is just in front of the object. At the time of (a) and (c), since the moving velocity of the object is fast, hand is not able to track the object. Since the tracking state of hand is same as that of hand or camera in fixed camera system,

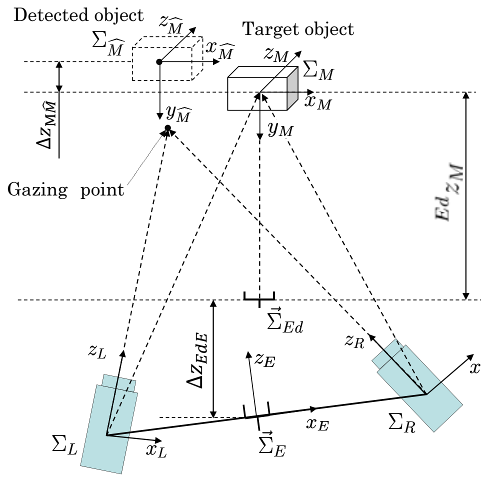

Fig. 8. Cameras' gazing point

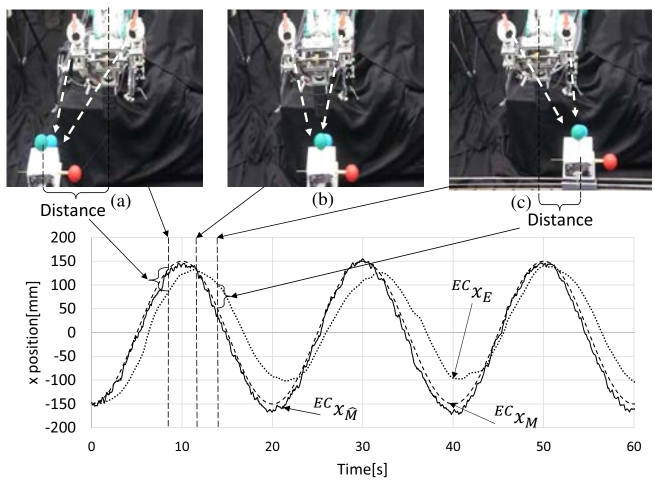

Fig. 9. Eye-vergence system and object position

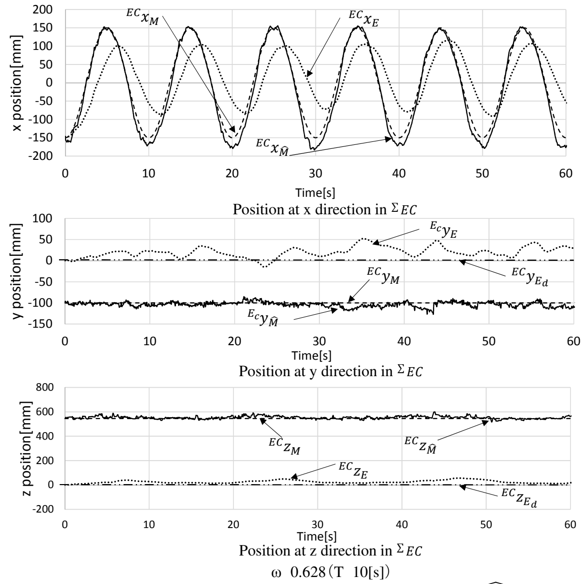

Fig. 10. Movements of actual object ^{M}x, detected object $^{\widehat{M}}x$ and end effector ^{E}x on the x,y and z directions in the center coordinate system of hand Σ_{EC}. The object's pose x, y, z, ε_1, ε_2 and ε_3 are recognized by camera.

$^{EC}x_E$ in the figure also represents the movement of hand or camera in fixed camera system. At this time, it is clear that the distance between the hand $^{EC}x_E$ and the object $^{EC}x_M$ on the x-axis direction is farther than that between the gazing point $^{EC}x_{\widehat{M}}$ and target object $^{EC}x_M$ of the camera. From the error between $^{EC}x_{\widehat{M}}$ and $^{EC}x_M$ it can be seen that it is easier for eye-vergence system to track the object than the fixed camera system.

b) Position tracking result and analysis of the tracking experiment: Because the object is reciprocating in the x direction, this time only the result of tracking at the x-axis is given and analyzed as shown in Fig.10. And at this time the movement cycle is 10 seconds ($\omega = 0.628$). As shown in Fig.10 when the cycle is 10 seconds it is clear that the motion of hand has delay against that of the object. And the deviation of the gazing point is smaller than that of hand. From the above, it can be seen that the trackability of the eye-vergence system is better than that of the end-effector.

C. Arc Swing Motion Experiment

1) Arc swing motion experiment condition: As shown in Fig.12 and Eq.(15) with the same set of horizontal tracking experiments the desired value of distance between object $\vec{\Sigma}_M$ and end-effector $\vec{\Sigma}_E$ is $^{E}x_M = 0$, $^{E}y_M = -100mm$, $^{E}z_M = 545mm$. And the relative orientation between object and end-effector is $\boldsymbol{\varepsilon} = \mathbf{0}$, i.e. in the process of tracking, always keep the x-y plane in $\vec{\Sigma}_E$ parallel to the x-y plane in $\vec{\Sigma}_M$. $\Sigma_T u$ is the coordinate system of turntable. And the turntable takes $\pm 20°$ reciprocal uniform rotation movement

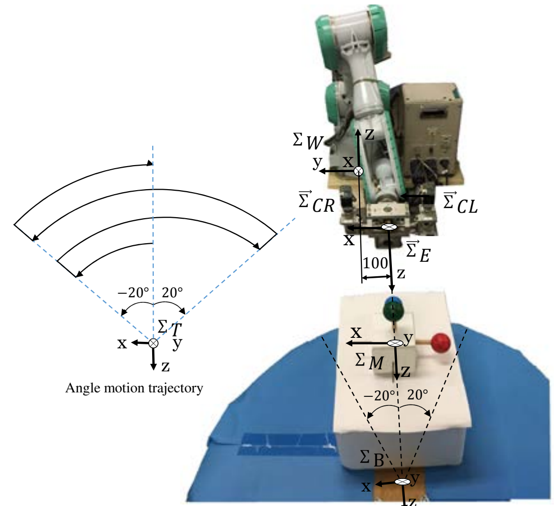

Fig. 11. Distribution of the initial state of each coordinate system and the angle motion trajectory

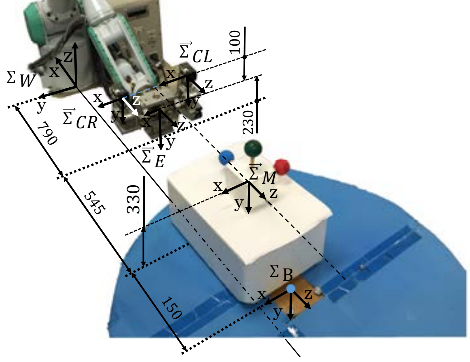

Fig. 12. Distribution of the initial state of object and visual-servoing system in orientation tracing experiment

around y-axis of Σ_B. The rotation function is

$$\theta = \begin{cases} -4.5t & t \in [0, 4.44)s \quad (16a) \\ -20 + 4.5(t - 4.44) & t \in [4.44, 13.32)s \quad (16b) \\ 20 - 4.5(t - 8.88) & t \in [13.32, 22.2)s \quad (16c) \\ -20 + 4.5(t - 22.2) & t \in (22.2, 26]s. \quad (16d) \end{cases}$$

At this speed it takes 80s to rotate one cycle, that means the angular velocity $\omega = \pm 2\pi/T = \pm 2\pi/80 = \pm 0.079$[rad/s]. As shown in Fig.12 similar to the lateral movement experiment, Σ_{EB} represent initial hand pose and also midpoint of round-trip tracking movements. The homogeneous transformation matrix from Σ_W to Σ_{EB} is:

$$^{W}\boldsymbol{T}_{EC} = \begin{bmatrix} 0 & 0 & -1 & -790[mm] \\ 1 & 0 & 0 & 0[mm] \\ 0 & -1 & 0 & 230[mm] \\ 0 & 0 & 0 & 1 \end{bmatrix} \quad (17)$$

During the experiment we just let object rotate around the y-axis of Σ_B as Eq.(16), therefore according to Eq.(1) and Eq.(2) the orientation $\boldsymbol{\varepsilon}_M$ of object is

$$\left[\varepsilon_{M1}, \varepsilon_{M2}, \varepsilon_{M3}\right]^T = sin\frac{\theta}{2}\left[0, 1, 0\right]^T = \left[0, sin\tfrac{\theta}{2}, 0\right]^T \quad (18)$$

shown as the dashed line in the Fig.13.

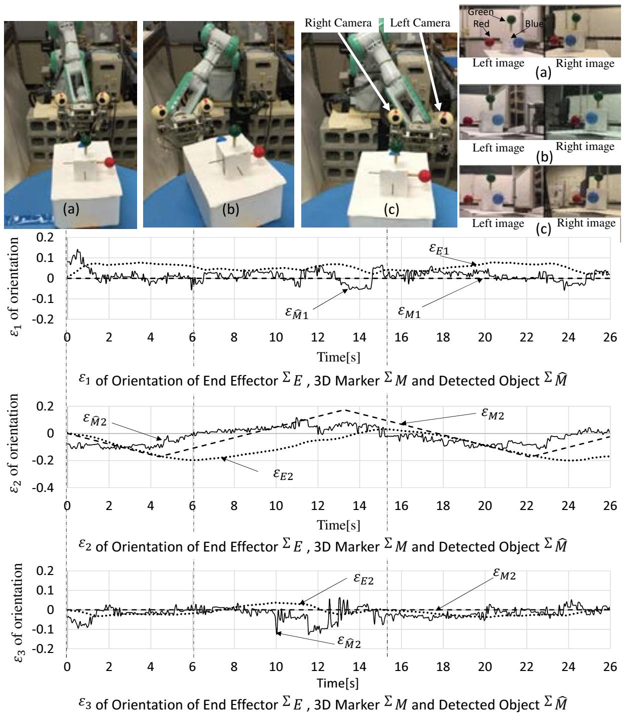

Fig. 13. Orientation tracking result of the turntable tracking experiment

2) Swing motion experiment results and analysis: In Fig.13 the three dashed lines represent the orientation ε_M of real target Σ_M. Orientation tracking result of the detected object $\vec{\Sigma}_{\widehat{M}}$ and end-effector $\vec{\Sigma}_E$ are also shown in Fig.13 as the solid line and dotted line respectively.

In Fig.13 the three pictures in the upper left corner show the status of three different times. The images obtained from cameras in the three moments are shown in the upper right corner respectively. The group of red, green and blue circles is the recognition result. (a) is the beginning status. And at the time of (b) the ε_{E2} of end-effector reaches the minimum value. At this moment manipulator moves to the far left position. And at the (c) moment the ε_{E2} reaches the maximum value. And manipulator moves to the far right position. However there is some delay with respect to the movement of object that has turned left and are not at the far right point. And it can be seen that although the background changes a lot, the target object is detected continually.

Same as the lateral motion tracking status of x, y and z the quaternion variation of $\varepsilon_{\widehat{M}}$ is more frequent than that of $\boldsymbol{\varepsilon_E}$. In Fig.13 the phases of $\varepsilon_{\widehat{M}1}$, $\varepsilon_{\widehat{M}2}$, $\varepsilon_{\widehat{M}3}$ are all earlier than that of $\vec{\Sigma}_E$.

Since the camera mass is smaller than manipulator, so the moment of inertia is also smaller than that of manipulator. Therefore it can adjust faster than manipulator. Another reason is that according to the control procedure the manipulator is controlled by the detecting result, although its effect is very small. Compared with the end-effector, giving the camera freedom can make the camera more quickly track the object during its transform of the orientation. And tracking error of each step in multi-step GA will not so large that manipulator can track the object stably.

V. CONCLUSION

In this paper the eye-vergence visual servoing controller of eye-vergence system have been described in detail. And by lateral and arc swing motion tracking experiment to the 3D marker with 6 degree of freedoms it has been analyzed that the recognition and control results of both of the position and orientation. Through the two experiments, especially by the second one we know the 3D pose tracking performance of the system. And they help us to further improve the system. Finally it is confirmed that not only position but also orientation trackability of the eye-vergence system have superior performances and are better than that of the end-effector (hand).

REFERENCES

[1] Hutchinson, Seth, Gregory D. Hager, and Peter I. Corke. “A tutorial on visual servo control.” Robotics and Automation, IEEE Transactions on 12.5, pp. 651-670, 1996.

[2] Song, Wei, Mamoru Minami, Yasushi Mae, and Seiji Aoyagi. “On-line evolutionary head pose measurement by feedforward stereo model matching.” In Robotics and Automation, 2007 IEEE International Conference on, pp. 4394-4400. IEEE, 2007.

[3] Stavnitzky, Jay, and David Capson. “Multiple camera model-based 3-D visual servo.” Robotics and Automation, IEEE Transactions on 16.6, pp. 732-739, 2000.

[4] Dune, Claire, Eric Marchand, and Christophe Leroux. “One click focus with eye-in-hand/eye-to-hand cooperation.” In Robotics and Automation, 2007 IEEE International Conference on, pp. 2471-2476. IEEE, 2007.

[5] Nishimura, Kenta, Sen Hou, Koichi Maeda, Mamoru Minami, and Akira Yanou. “Analyses on on-line evolutionary optimization performance for pose tracking while eye-vergence visual servoing.” In 2013 IEEE International Conference on Mechatronics and Automation, pp. 698-703. IEEE, 2013.

[6] Tian, Hongzhi, Yu Cui, Mamoru Minami, and Akira Yanou. “Frequency response experiments of eye-vergence visual servoing in lateral motion with 3D evolutionary pose tracking.” Artificial Life and Robotics, pp. 1-8, 2016.

[7] Cucchiara, Rita, C. Grana, Metal Piccardi, and A. Prati. “Statistic and knowledge-based moving object detection in traffic scenes.” In Intelligent Transportation Systems, 2000. Proceedings. 2000 IEEE, pp. 27-32. IEEE, 2000.

[8] Myint, Myo, Mamoru Minami, Kenta Yonemori, Khin Lwin, Akira Yanou, “Dual-eyes Visual-based Sea Docking for Sea Bottom Battery Recharging.” MTS/IEEE OCEANS’ 16, September 19-23, 2016.

[9] Myint, Myo, Kenta Yonemori, Akira Yanou, Khin Nwe Lwin, Mamoru Minami, and Shintaro Ishiyama. “Visual Servoing for Underwater Vehicle Using Dual-Eyes Evolutionary Real-Time Pose Tracking.” Journal of Robotics and Mechatronics 28, no. 4, pp. 543, 2016.

[10] Song, Wei, Mamoru Minami, and Seiji Aoyagi. “On-line stable evolutionary recognition based on unit quaternion representation by motion-feedforward compensation.” International Journal of Intelligent Computing in Medical Sciences & Image Processing 2.2, pp. 127-139, 2008.

[11] Maeda, Koichi, Mamoru Minami, Akira Yanou, Hiroaki Matsumoto, Fujia Yu, and Sen Hou. “Frequency response experiments of 3-d pose full-tracking visual servoing with eye-vergence hand-eye robot system.” In SICE Annual Conference (SICE), 2012 Proceedings of, pp. 101-107. IEEE, 2012.